Oil & Gas Science and Technology - Rev. IFP Energies nouvelles **74**, 83 (2019)
© X. Ma et al., published by IFP Energies nouvelles, 2019
https://doi.org/10.2516/ogst/2019055

Available online at:
ogst.ifpenergiesnouvelles.fr

Subsurface Fluid Injection and Energy Storage
Q. Li, M. Kühn (Guest editors)

REGULAR ARTICLE OPEN ACCESS

Geochemical modeling of changes in caprock permeability caused by CO_2–brine–rock interactions under the diffusion mechanism

Xin Ma[1,2], Guodong Yang[3,*], Xufeng Li[1,2], Ying Yu[4], and Jianxing Dong[5]

[1] Center for Hydrogeology and Environmental Geology Survey, CGS, Baoding 071051, China
[2] Key Laboratory of Carbon Dioxide Geological Storage of China Geological Survey, Baoding 071051, China
[3] School of Resource and Environmental Engineering, Wuhan University of Science and Technology, Wuhan 430081, China
[4] School of Environmental Studies, China University of Geosciences, Wuhan 430074, China
[5] Chengdu Hydrogeology and Engineering Geology Center, Sichuan Bureau of Geology and Mineral Resources, Chengdu 610081, China

Received: 19 May 2019 / Accepted: 11 October 2019

Abstract. Geologic Carbon Sequestration (GCS) has been widely considered as a significant means for reducing CO_2 emissions to address global climate change. The caprock sealing plays a key role in determining permanence and security of carbon dioxide (CO_2) storage in geologic formations. This study presents geochemical modeling of CO_2–brine–rock interactions in a deep saline aquifer in the Jianghan Basin, which is a potential target for CO_2 injection and geological storage. A one-dimensional model was developed to investigate the changes in caprock permeability caused by CO_2–brine–rock interactions under the diffusion mechanism. The results show that the dissolution of K-feldspar and albite plays a key role in the variation of caprock permeability, which makes permeability increased by 60% at the bottom of caprock. The caprock permeability is increased with temperature by enhancing the minerals dissolution of caprocks. In addition, the common-ion effect generated by the increased salinity inhibits the minerals dissolution in caprock.

1 Introduction

Greenhouse effect mainly due to anthropogenic CO_2 emissions has caused a series of global environmental problems, CO_2 emission reduction has become hot issues of general concern [1–3]. It is generally accepted that CO_2 geological storage is the most promising method for reducing atmospheric CO_2 emissions [4–8]. However, the greatest concern is the CO_2 storage security. Local CO_2 leakage could lead to acidification of groundwater, which seriously cause suffocation of surface creatures. Also, it could cause the increase of CO_2 concentration in atmosphere, and even lead to gas explosion [9–12]. As a barrier to prevent CO_2 leakage, caprock has become the focus of research.

Many experimental, modeling and field studies have been conducted to evaluate the feasibility and safety of CO_2 geological storage. Siirila-Woodburn *et al.* have presented risk maps of a comprehensive assessment of CO_2 leakage risk using plugged and abandoned wellbores [13]. The occurrence of CO_2 leakage from the reservoir may strongly affect the sealing capability of the caprock [14]. In deep saline aquifers, the convective mixing mechanism and its effectiveness are critical for permanent CO_2 geological storage [15]. Threshold pressure and permeability also play a critical role in the implementation of CO_2 geological storage [16]. In order to decrease the buoyancy effect on CO_2 geological storage, Uemura *et al.* have proposed a new technique for geological sequestration of CO_2 using nanosized CO_2 droplets which can be trapped in a porous silica medium [17]. Based on China Shenhua CCS project, some studies have found that very small amount of CO_2 will enter into the caprock from the reservoir during long-term storage process, resulting in changes in caprock permeability. They also have evaluated the leakage risk with the updated Oldenburg's Screening and Ranking Framework (SRF) [18–20]. These results show that the reaction of CO_2–water–caprock minerals induces the mineral alteration, which affect the porosity, permeability, capillary pressure and mineral wettability of the caprock. While this effect largely depends on mineral composition of the caprock and the migration mechanisms of CO_2. Different mechanisms of CO_2 migration have different effects on the caprock seal capacity. It is need to study CO_2–brine–rock interactions under different migration mechanisms, which is conducive to the further research and widely development of CO_2 geological storage project in the future.

* Corresponding author: ygdguodong@126.com

This is an Open Access article distributed under the terms of the Creative Commons Attribution License (https://creativecommons.org/licenses/by/4.0), which permits unrestricted use, distribution, and reproduction in any medium, provided the original work is properly cited.

Many researchers have studied CO_2–brine–rock interactions on caprock permeability based on many CO_2 geological storage sites. Luquot and Gouze have found that the brine is almost saturated with CO_2 near the injection well. The fluid displayed lower values and higher divalent cation concentrations due to rock dissolution along the fluid pathway at a distance of the injection well [21]. Aquifer pH and Total Dissolved Solids (TDS) were influenced by CO_2 leakage, which would affect the reservoir physical parameters (mainly porosity and permeability) [22]. The 2D reactive transport simulations conducted by Wolf *et al.* have found a distinct inner region of 2000 m radial distance under the dominating impact of dissolved CO_2 [23]. Near the injection well, increasing the stress which impact mainly depends on the dissolution regime inhibited the permeability enhancement, increasing the injected volume required to reach a certain permeability [24]. Wang *et al.* have predicted a maximum 3.2% permeability increase of the reservoir and a maximum 1.1% permeability increase of the caprock after 1000 years of exposure to CO_2-rich brine under the convection mechanism [25]. The results also show that potential geochemically changes to the porosity and permeability of host CO_2 storage and sealing formation rock would improve CO_2 storage capacity [26]. Some of the existing experimental data and/or thermodynamic models were about the effect of capillary pressure on the behavior of the CO_2–water–caprock system. Although many experiments have been performed outside porous media or in highly permeable cores, the capillary-pressure effects are negligible. Consequently, thermodynamic models have been optimized/tuned based on the available experimental data in bulk. While the migration mechanisms of CO_2 into the caprock include convection mechanism (CO_2 filtering into caprock by breaking through capillary pressure) and diffusion mechanism (CO_2 diffusing into caprock by dissolving in water). Under the diffusion mechanism, although CO_2 gas does not break through the capillary pressure into the caprock, it would also lead to CO_2 dissolution in the caprock water during the long-term CO_2 geological sequestration, which would have an impact on the caprock seal capacity. However, few of the existing experimental data and/or thermodynamic models including the effect of the diffusion mechanism (at a distance of the injection well) on the behavior of the CO_2–water–caprock system. The changes in caprock permeability caused by CO_2–brine–rock interactions under the diffusion mechanism are not fully understood.

In this study, we have developed a one-dimensional vertical model using geochemical modeling software of TOUGHREACT based on the available site-specific data in the Jianghan Basin, China. Jianghan Basin is rich in oil and saline water resources. This area has economic and social ties to the oil and gas industry. The matching between carbon sources and sinks is relatively good in this region, since clusters of large CO_2 emitters have been identified both in Wuhan and Jingzhou. According to the potential evaluation of CO_2 geological storage conducted by China Geological Survey, the CO_2 storage potential of the Jianghan Basin can reach up to 1700 Mt. Preliminary studies indicate that Jianghan Basin is suitable for CO_2 enhanced oil recovery and saline water recovery [27]. The objective of this study is to investigate the CO_2–water–rock geochemical reactions on caprock permeability under the case of diffusion mechanism. The parameters which may affect these geochemical processes are also analyzed. In this paper, diffusion mechanism means that there is no flow in the system and only diffusion plays a role in CO_2 transport. The CO_2 enters into the caprock mainly in its dissolved form. The results of this study could provide a theoretical basis for the safety evaluation of caprock.

2 Numerical simulation methods

2.1 Simulation tool

TOUGHREACT [28] was developed by introducing reactive geochemistry into the framework of the existing multi-phase fluid and heat flow code TOUGH2 [29]. TOUGHREACT Version 2.0 can be applied to one-, two- or three-dimensional porous and fractured media with physical and chemical heterogeneity. The code can accommodate any number of chemical species presented in the liquid, gas and solid phases [30].

In TOUGHREACT, for the rock matrix, it is given as a relation to porosity, using a simplified form of the Carman-Kozeny equations (1) and (2). Matrix permeability changes are calculated from changes in porosity using ratios of permeability calculated from the Carman-Kozeny relation, and ignoring changes in grain size, tortuosity and specific surface area as follows [30]:

$$k = k_0 \frac{(1-\phi_0)^2}{(1-\phi)^2}\left(\frac{\phi}{\phi_0}\right)^3, \tag{1}$$

$$\phi = 1 - \sum_{m=1}^{nm} \mathrm{fr}_m - \mathrm{fr}_u, \tag{2}$$

where,

k – current permeability (m^2),
k_0 – initial permeability (m^2),
ϕ – current porosity (%),
ϕ_0 – initial porosity (%),
nm – the number of minerals,
fr_m – volume fraction of mineral m in the rock (%),
fr_u – volume fraction of the unreaction rocks (%).

TOUGHREACT has been developed as a comprehensive non-isothermal multi-component reactive fluid flow and geochemical transport simulator to geological and environmental problems. A number of subsurface thermo-physical-chemical processes are considered under various thermohydrological and geochemical conditions of pressure, temperature, water saturation, and ionic strength [30]. It has been widely applied to numerical simulation study of different geological and environmental issues, in which the geological storage of CO_2 is one of its main purposes.

2.2 Geological settings of the study area

The Jianghan Basin lies in the south-central part of the Hubei Province, west to Yichang city, east to Yingcheng city, and south to Honghu city, north to Jingzhou city. It is a typical salt lake rift basin developed on the Mid-Yangtze Paraplatform during the Cretaceous and Tertiary Period, covering an area of 36 350 km^2. It is tectonically located in the central part of the Mid-Yangtze Depression in Yangtze Paraplatform, west to Western Hubei fold belt, east to Wuhan-Tongshan fold belt, north to Bahong fold belt and south to Jianghan fold belt. The Early Cretaceous Basement of the Jianghan Basin is a double-deck structure consisting of Proterozoic metamorphic rocks in the lower part and sedimentary rocks deposited from Sinian to Mesozoic Jurassic in the upper part acting as the caprock of the Mid-Yangtze depression of Yangtze Paraplatform. Late Yanshan and Xishan tectonic movements occurred in Cretaceous and Paleogene play a dominant role in its evolution and development. The development of Jianghan Basin divides into seven different phases controlled by tectonic movements which can be grouped into two tectonic cycles characterized by tension crack-rift-depression (Fig. 1). In addition, with the controlling of the northeast and northwest basement faults, the basin forms eight-depression and four-uplift (or low uplift) structural pattern.

The reservoirs of Jianghan Basin include sandstone, globulitic marl, fractured mudstone and basalt, with sandstone as the major. The caprocks involve mudstone and gypsum-slat bed. The sandstone aquifers and overlying mudstone and gypsum-salt bed represent numerous pairs of reservoirs and seals. Xingouzui Formation is the predominant petroliferous and saline sandstone reservoirs, which are the most promising reservoir and seal pairs for CO_2 storage (Table 1).

There are three delta sand bodies (Hanchuan, Hougang and Mashan) in the Paleogene Xingouzui Formation, distributing in the north of Jianghan Basin from west to east, and connecting with each other forming a reservoir development belt, which becomes thinner from north to south sand layer. The distribution area of the sand bodies is 11 000 km^2, the thickness is generally from 20 m to 140 m, and the maximum thickness is 237 m. The lithology is mainly composed of siltstone, of which the average porosity and permeability are 17% and 9.8×10^{-14} m^2, respectively. The depth of the Xingouzui Formation ranges from 1000 m to 2000 m, with the shallowest depth is 989.4 m, which can ensure the supercritical state of CO_2. When the depth is more than 1000 m, the TDS of the water basically does not change with depth, usually from 10×10^4 to 26×10^4 mg/L (0.1–0.26 as the mass fraction of salinity) [31].

The mudstone, gypsum and salt rock are the main caprocks of the Cretaceous-Paleogene in the Jianghan Basin, in which the mudstone is the main caprock in this area. The main mineral components of mudstone are clay minerals, while non-clay minerals are mainly consisted of quartz, feldspar, gypsum, etc., and a small quantity of calcite and pyrite [32]. Composition of clay minerals of the area is shown in Table 2.

Table 3 shows the physical parameters of the mudstone caprocks from the Cretaceous to the Paleogene in the Jianghan Basin. It can be seen that the porosity of the mudstone

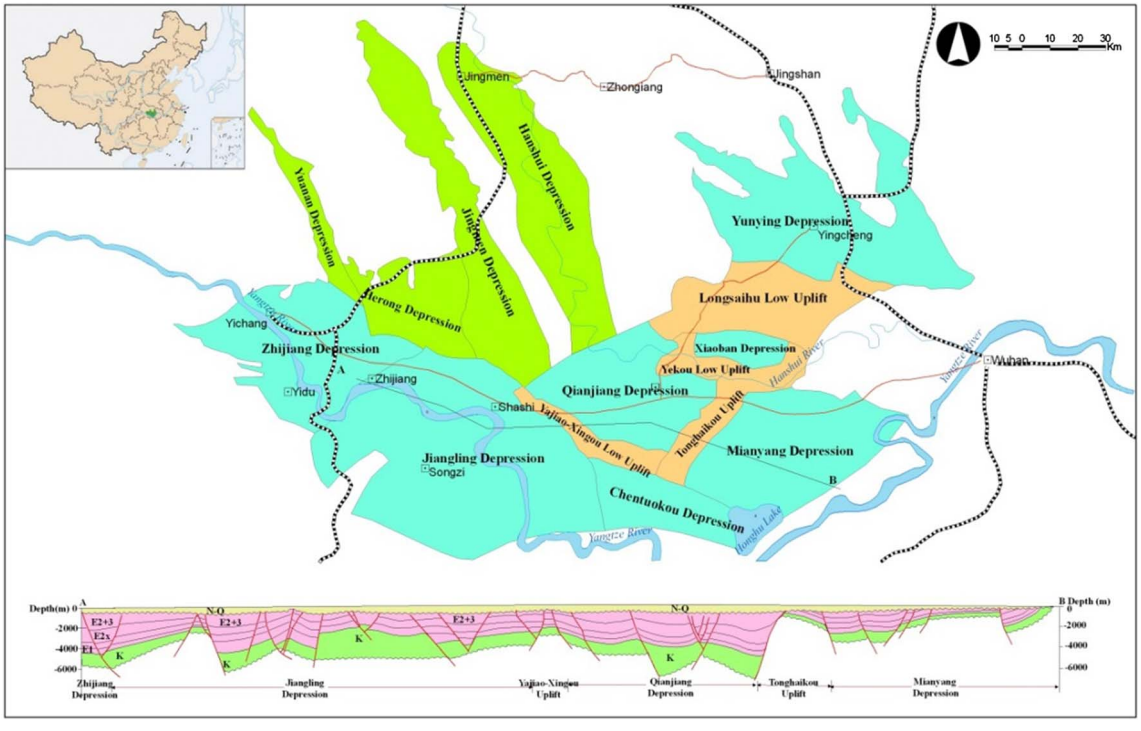

Fig. 1. Structure map of the Jianghan Basin.

Table 1. Reservoir and seal pairs of Xingouzui formation in Jianghan Basin.

Formation			Thickness (m)	Lithologic character	Reservoir	Seal
Xingouzui Formation	Upper		200~600	Red mudstone with sandstone		
		Gypsum	5~20	Grey argillaceous gypsum and white gypsum		
		Sandstone 1	50~150	Red-grey mudstone and sandstone		
	Lower	Sandstone 2	100~250	Grey mudstone with marl and sandstone		
		Mudstone	100~250	Grey mudstone with gypsum-bearing mudstone		
		Sandstone 3	100~250	Red-grey mudstone and sandstone		

Table 2. Clay mineral composition of mudstone (% of mass).

Well depth (m)	Illite (%)	Chlorite (%)	Chlorite/ smectite mixed (%)	Illite/ smectite mixed (%)	Kaolinite (%)
<1400	67.16	7.61	0.44	23.16	1.39

Table 3. Physical parameters of the mudstone caprocks in the Jianghan Basin from the Cretaceous to the Paleogene (average value).

Structural pattern	Porosity (%)	Permeability (10^{-15} m^2)
Qianjiang depression	6.01	0.155
Xiaoban depression	3.96	0.341
Mianyang depression	8.68	0.271
Yajiao-xingou low uplift	9.94	0.113
Yuekou low uplift	8.53	0.045
Tonghaikou uplift	7.2	1.180

The data in Table 3 comes from Petroleum Geology of China (Vol. 9): Jianghan Oilfield [34] and the literature [32].

caprock is less than 10%, with average porosity is 7.5%, and the average permeability is 3.0×10^{-16} m^2.

2.3 Model setup

A vertical one dimensional (1D) model is developed (Fig. 2), the 61.4 m column is divided into a total of 41 layers in the vertical direction [14]. The grid cells of the other two directions are 1 m. The mesh generation is shown in Table 4. The volumes of the reservoir and top grid of caprocks are set as 10^{10} m^3 and 10^{60} m^3, respectively. This setting causes only minor changes in reservoir parameters in TOUGHREACT, while the top grid parameters of the caprock are stable. This setting not only maintains the relatively constant pore pressure and CO_2 gas saturation of the reservoir, but also considers the effect of geochemical reactions on caprocks. The upper part of caprocks is an open boundary to ensure that CO_2 can spread to the upper more realistically. This model describes the situation of CO_2 entering the caprock under the diffusion mechanism.

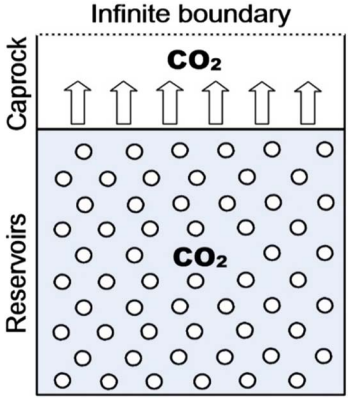

Fig. 2. Sketch of the 1D vertical model.

Table 4. Mesh generation of one-dimensional model.

Rock formation	Vertical mesh number	Mesh thickness (m)	Note
Caprock	1	2.0	Infinite boundary
Caprock	14	2.0	
Caprock	17	1.0	
Caprock	1	0.9	
Caprock	1	0.8	
Caprock	1	0.7	
Caprock	1	0.6	
Caprock	1	0.5	
Caprock	1	0.4	
Caprock	1	0.3	
Caprock	1	0.2	
Reservoir	1	10.0	Huge volume

2.4 Parameters selection

According to the geological conditions of the Jianghan Basin, the sandstone of Xingouzui Formation is selected as the reservoir, with the depth is 1000 m [33]. The mudstone

Table 5. Hydrogeological parameters used in the simulations.

Parameters	Formation	
	Reservoir	Caprock
Porosity	0.17	0.075
Horizontal permeability (m^2)	1.0×10^{-13}	3.0×10^{-16}
Vertical permeability (m^2)	1.0×10^{-14}	3.0×10^{-17}
Pore compressibility (Pa^{-1})	4.5×10^{-10}	4.5×10^{-10}
Rock grain density (kg/m^3)	2600	2600
Formation heat conductivity (W/m °C)	2.51	2.51
Rock grain specific heat (J/kg °C)	920	920
Temperature (°C)	47	47
Salinity (mass fraction)	0.10	0.10
Pressure (bar)	101	101
Gas saturation	0.50	0.00
Relative permeability		
Liquid: Van Genuchten function		
$k_{rl} = \sqrt{S^*}\left\{1 - (1 - [S^*]^{1/m})^m\right\}^2$	$S^* = (S_l - S_{lr})/(1 - S_{lr})$	
S_{lr}: residual water saturation	$S_{lr} = 0.30$	
m: exponent	$m = 0.457$	
Gas: Corey		
$k_{rg} = (1 - \hat{S})^2 (1 - \hat{S}^2)$	$\hat{S} = (S_l - S_{lr})/(S_l - S_{lr} - S_{gr})$	
S_{gr}: residual gas saturation	$S_{gr} = 0.05$	
Capillary pressure		
Van Genuchten function		
$P_{cap} = -P_0([S^*]^{-1/m} - 1)^{1-m}$	$S^* = (S_l - S_{lr})/(1 - S_{lr})$	
S_{lr}: residual water saturation	$S_{lr} = 0.00$	
m: exponent	$m = 0.457$	
P_0: strength coefficient	$P_0 = 19.61$ kPa	$P_0 = 6.25$ kPa

of Xingouzui Formation is selected as the caprock. Since the hydrostatic pressure gradient is 10 MPa/km, the initial hydrostatic pressure of the reservoir before CO_2 injection is 10.1 MPa, and the hydrostatic pressure distribution in the cap rock can be obtained according to the pressure gradient. The annual average temperature at the surface is 16 °C and the geothermal gradient is about 3.1 °C/100 m in this study area [34]. It can be calculated that the reservoir temperature is 47 °C (no temperature change is considered in the simulation). The specific parameter settings are shown in Table 5.

In the model, the vertical permeability of the reservoir is taken as 1/10 of the horizontal permeability [14]. The horizontal permeability of the reservoir is set as 1×10^{-13} m^2, and the vertical permeability is 1×10^{-14} m^2. Take the arithmetic mean value of the mudstone permeability (Tab. 3) as the horizontal permeability of the caprock, which is 3.0×10^{-16} m^2. Therefore, the vertical permeability of the caprock is set as 3.0×10^{-17} m^2. The porosity of the reservoir is set at 17%, while the porosity of the caprock is set at 7.5% from the arithmetic mean of the data listed in Table 3. The salinity of the formation water is 0.10. The parameters for calculating capillary pressure and relative permeability are quoted from the literature [14].

In order to characterize the transition of CO_2 into the caprock under the diffusion mechanism, the pore pressure in the reservoir is set as 10.1 MPa and the Sg (CO_2 gas saturation) is set as 0.5 [14]. The caprock water pressure is the initial hydrostatic pressure, and Sg (CO_2 gas saturation) is zero.

The mineral compositions of the reservoir and caprock are shown in Table 6. When the primary mineral composition of the caprock is set, assuming the clay minerals in the mudstone caprocks accounted for 80% of the total. The volume fractions of four clay minerals (illite, kaolinite, smectite and chlorite) are obtained from the proportional relationships. Because 80% of the proportion is the estimated value, the sensitivity analysis is conducted by setting the ratio of 70% and 90%, respectively. The difference on the numerical results is small, which does not affect the results. Thermodynamics data of the minerals used in the simulation mainly referred to relevant literatures [35, 36].

The initial concentrations of the hydrogeological components of the reservoir and caprock in the model are obtained by a 100-year chemical reaction of the reservoir and caprock minerals with water salinity of 0.10 as shown in Table 7.

Table 6. Initial mineral volume fractions and possible secondary mineral phases used in the simulations [31].

Mineral classification	Mineral name	Chemical composition	Reservoirs (volume fraction)	Caprock (volume fraction)
Clay minerals	Illite	$K_{0.6}Mg_{0.25}Al_{1.8}(Al_{0.5}Si_{3.5}O_{10})(OH)_2$	0.15	0.653
	Kaolinite	$Al_2Si_2O_5(OH)$	0.03	0.0111
	Smectite-Ca	$Ca_{0.145}Mg_{0.26}Al_{1.77}Si_{3.97}O_{10}(OH)_2$	0	0.0696
	Chlorite	$Mg_{2.5}Fe_{2.5}Al_2Si_3O_{10}(OH)_8$	0.10	0.064
Non-clay mineral	Quartz	SiO_2	0.35	0.08
	K-feldspar	$KAlSi_3O_8$	0.20	0.028
	Albite	$NaAlSi_3O_8$	0	0.032
	Anhydrite	$CaSO_4$	0	0.04
	Calcite	$CaCO_3$	0.10	0.008
	Pyrite	FeS_2	0	0.004
	Oligoclase	$CaNa_4Al_6Si_{14}O_{40}$	0.05	0
	Hematite	Fe_2O_3	0.005	0
	Siderite	$FeCO_3$	0	0
	Ankerite	$CaMg_{0.3}Fe_{0.7}(CO_3)_2$	0	0
	Dawsonite	$NaAlCO_3(OH)_2$	0	0
	Magnesite	$MgCO_3$	0	0
	Dolomite	$CaMg(CO_3)_2$	0	0
	Halite	NaCl	0	0

Table 7. Initial total dissolved component concentrations for reactive transport simulations.

Component	Concentration of reservoir (mol/kg H_2O)	Concentration of caprock (mol/kg H_2O)
Ca^{2+}	5.945×10^{-3}	6.233×10^{-2}
Mg^{2+}	1.108×10^{-4}	7.048×10^{-4}
Na^+	2.014	1.710
K^+	1.362×10^{-4}	6.633×10^{-5}
Fe	7.440×10^{-5}	8.813×10^{-4}
SiO_2 (aq)	2.501×10^{-3}	5.173×10^{-4}
C	1.458×10^{-2}	5.182×10^{-3}
SO_4^{2-}	1.099×10^{-16}	6.216×10^{-2}
Al^{3+}	1.983×10^{-10}	1.600×10^{-9}
Cl^-	2.012	1.710

Notes. Iron is the sum of Fe^{2+}, Fe^{3+} and their related complexities. Carbon is the sum of CO_2 (aq), CH_4 (aq), and their related species such as HCO_3^- and acetic acid (aq). Sulfur is the sum of sulfate and sulfide species.

3 Results

3.1 Migration of intruded CO_2 in the caprock

CO_2 was presented in the dissolved and supercritical states after entering the reservoir. Near the injection well, the supercritical CO_2 had a strong penetrability because of the dual effects of injection pressure and formation hydrostatic pressure. At a distance from the injection well, the transport mechanism of CO_2 was main diffusion with weak convection and penetration. CO_2 mainly existed in the dissolved state and the migration mechanism was mainly diffusion.

Under the dual mechanisms of convection and diffusion, the supercritical CO_2 entered the caprock, making the concentration of dissolved CO_2 in the caprock change greatly, and reached 1.3 mol/kg H_2O in the 5000 years (Fig. 3a). However, only under the diffusion mechanism, the supercritical CO_2 could not enter the caprock, so that the amount of CO_2 in the caprock greatly reduced, and the dissolved CO_2 distributed only in the range of about 2 m at the bottom of the caprock (Fig. 3b).

Figure 4a shows the dissolved CO_2 entering the caprock in the case of diffusion mechanism. If the diffusion coefficient is set to 0, no dissolved CO_2 enter the caprock (Fig. 4b). It can be concluded that diffusion is the only mechanism promoting CO_2 into the caprock in the absence of pressure. Diffusion is an objective existence, and the following are the effects of CO_2–water–rock geochemical reaction on the closure of the caprock considering the diffusion effect.

3.2 Variation in pH value and caprock permeability in the case of diffusion mechanism

The spatial variations of pH value in the caprock water are shown in Figure 5. It can be seen that although the supercritical CO_2 does not enter the caprock, the pH of the caprock is affected within 2.3 m above the bottom of the caprock, indicating that the dissolved CO_2 migrate upward

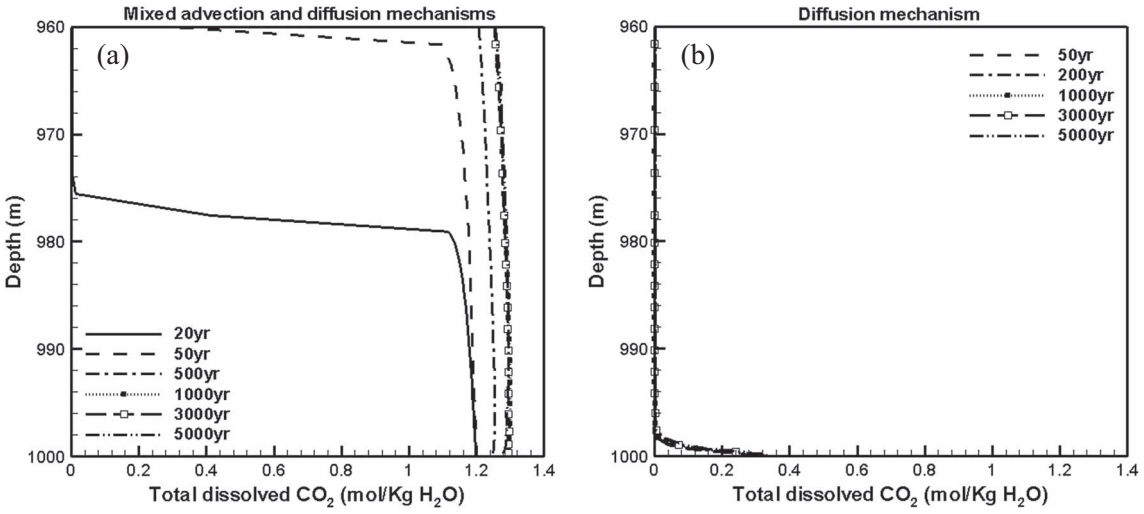

Fig. 3. The solubility of CO_2 under different migration mechanism.

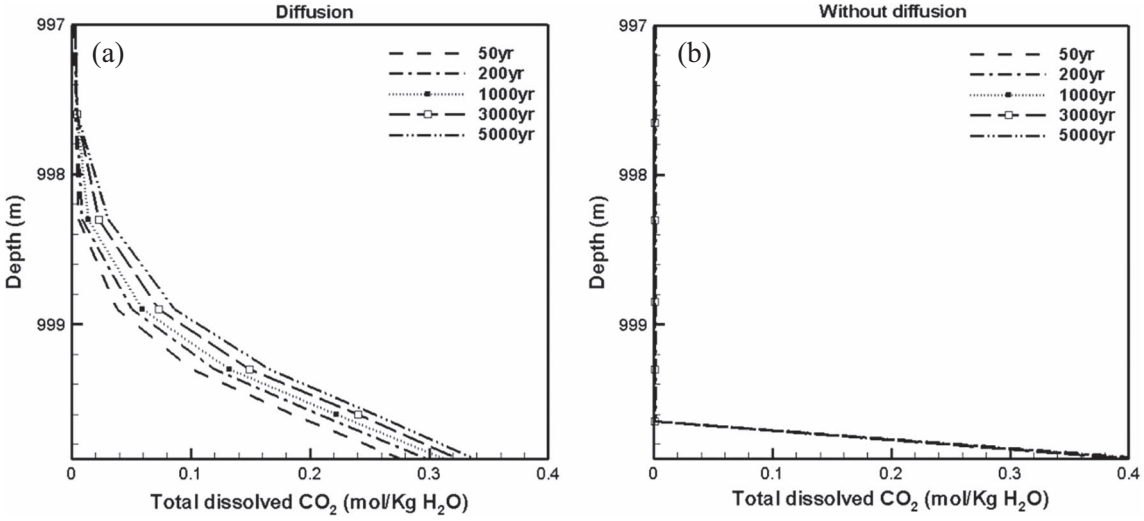

Fig. 4. Effect of diffusion on dissolved CO_2 in caprock.

and reduce the pH of the water. As an important indicator of water chemistry, pH change was bound to break the original water–rock reaction balance, leading to caprock mineral dissolution or precipitation, thus affecting the permeability of the caprock.

In Figure 6, the dissolved CO_2 diffused into the caprock and strongly dissipated in the rocks under the diffusion mechanism. The changes in permeability of the caprock gradually decreased from the bottom upwards until the permeability was not affected. The increase in the bottom permeability was the largest, from 3.0×10^{-17} m^2 to 4.8×10^{-17} m^2, which was about 60% higher than the initial. CO_2 diffused overall about 2.3 m in 5000 years.

The change in permeability was mainly determined by the combined effect of the dissolution and precipitation of minerals in the caprock (Eqs. (1) and (2)). K-feldspar and albite always dissolved in 5000 years (Fig. 7), which would cause the increase in permeability of the caprock. In the model, quartz mainly precipitated, however, the changes of quartz content in volume fraction during 5000 years were very little compared with the changes of K-feldspar and albite. It can be seen that the dissolution of K-feldspar and albite was the main reason for the increase in permeability of the caprock.

3.3 Impact of mineral composition on caprock permeability

Under the effect of diffusion, the bottom of the caprock suffered a strong dissolution, and the permeability of the bottom was increased by 60%. From the Kozeny-Carman

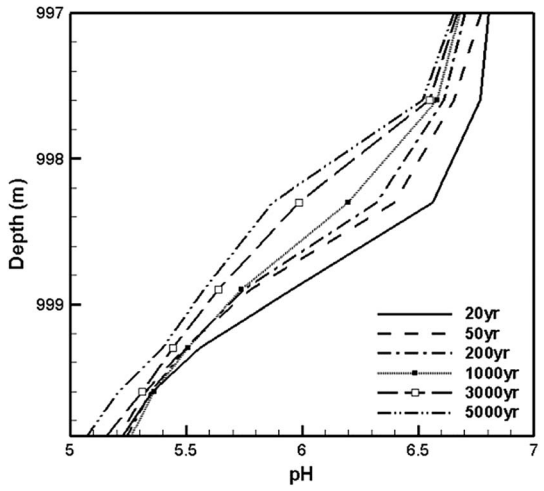

Fig. 5. Changes in pH of the caprock water.

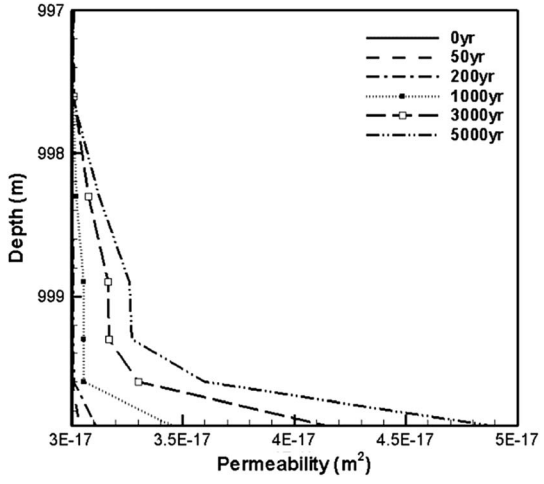

Fig. 6. Changes in caprock permeability.

equation, the change in permeability was mainly determined by the combined effect of the dissolution and precipitation of minerals in the caprock. The results showed that minerals such as calcite, chlorite, K-feldspar, and albite in the caprock were dissolved in the process of long-term CO_2–water–rock geochemical reactions, and the sensitivity analysis for these minerals was necessary.

During the simulation, the content of one or several dissolved (soluble) minerals was set to zero without changing the content of other minerals (a. calcite content was 0; b. chlorite content was 0; c. K-feldspar content was 0; d. albite content of 0; e. K-feldspar, albite content were 0; f. base case). The results of the sensitivity analysis of the main dissolved minerals are shown in Figure 8. It can be seen that the increase in permeability was greater in the absence of calcite, indicating that the dissolution of the caprock was irrelevant to calcite dissolution. In the absence of chlorite, K-feldspar and albite, the dissolution of the caprock decreased, indicating that the dissolution of the caprock was related to the dissolution of these three minerals and the effect of K-feldspar and albite was much larger than that of chlorite. The caprock dissolved least in the absence of K-feldspar and albite, indicating that such a strong dissolution phenomenon mainly caused by the K-feldspar and albite dissolution.

3.4 Impact of temperature on caprock permeability

In order to study the effect of temperature on the dissolution of the caprock, we changed the temperature in the original model to 57 °C (the original temperature was 47 °C). As can be seen in Figures 9a and 9b, the dissolution of the caprock was enhanced in 5000 years after the temperature was increased by 10 °C.

The kinetic rate constant k in equation (3) only considers the well-studied mechanism in pure H_2O (at neutral pH). Dissolution and precipitation of minerals are often catalyzed by H^+ (acid mechanism) and OH^- (base mechanism). For many minerals, the kinetic rate constant k includes each of these three mechanisms [37, 38].

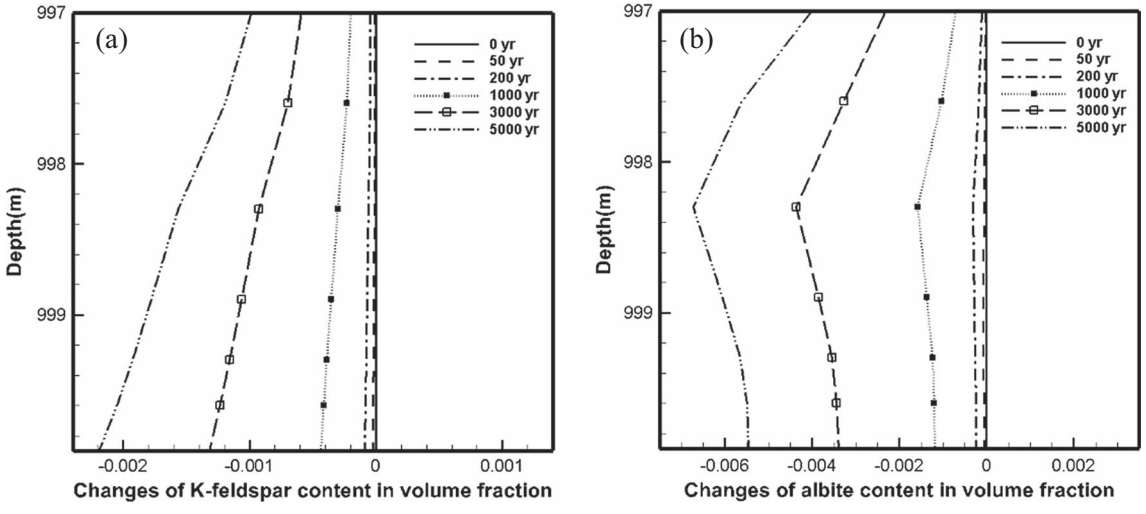

Fig. 7. Changes of K-feldspar, albite content in the case of diffusion mechanism.

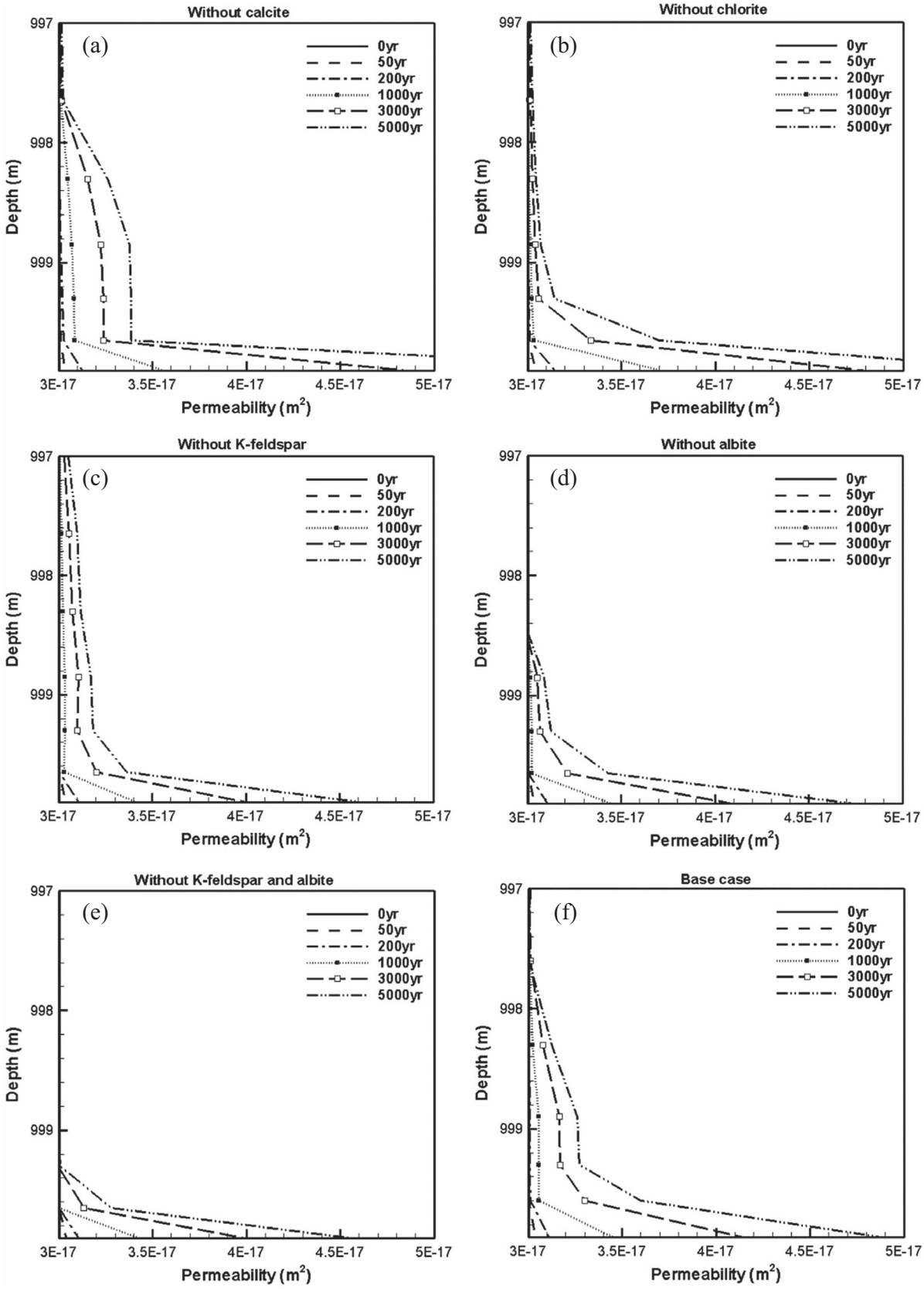

Fig. 8. Changes in caprock permeability for different mineral compositions.

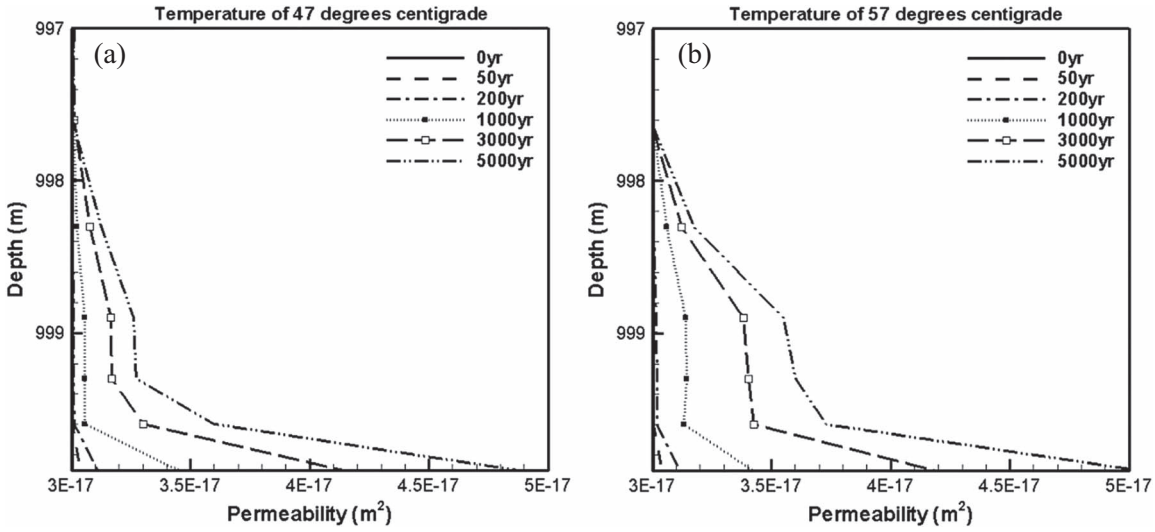

Fig. 9. Changes in caprock permeability at the temperatures of 47 °C and 57 °C.

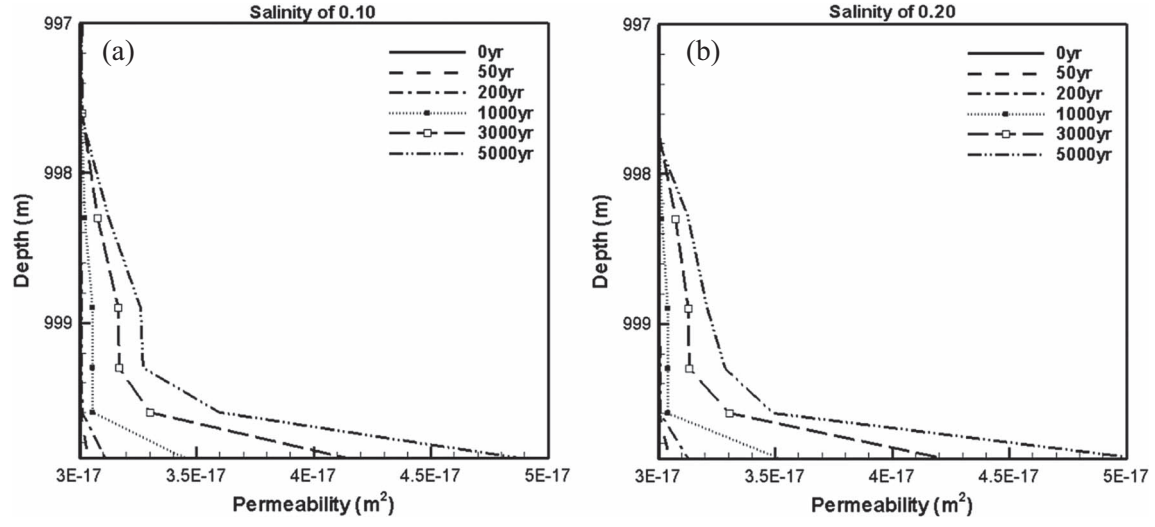

Fig. 10. Effect of salinity on permeability of caprock.

$$k = k_{25}^{\mathrm{nu}} \exp\left[\frac{-E_a^{\mathrm{nu}}}{R}\left(\frac{1}{T}-\frac{1}{298.15}\right)\right] + k_{25}^{\mathrm{H}} \times \exp\left[\frac{-E_a^{\mathrm{H}}}{R}\left(\frac{1}{T}-\frac{1}{298.15}\right)\right] a_H^{n_H} + k_{25}^{\mathrm{OH}} \times \exp\left[\frac{-E_a^{\mathrm{OH}}}{R}\left(\frac{1}{T}-\frac{1}{298.15}\right)\right] a_{\mathrm{OH}}^{n_{\mathrm{OH}}}, \quad (3)$$

where superscripts or subscripts nu, H, and OH indicate neutral, acid and base mechanisms, respectively; a is the activity of the species; and n is power term (constant). E_a is the activation energy, k_{25} is the rate constant at 25 °C, R is gas constant, T is absolute temperature. Notice that parameters θ and η are assumed the same for each mechanism.

It can be seen from the equation that kinetic rate constant increases with the rising of temperature, and when the temperature increases, the mineral dissolution rate also increases. Under the domination of mineral dissolution in the mineralization reaction, the dissolution further increases as the caprock permeability increases.

3.5 Impact of salinity on caprock permeability

The formation water salinity also affects the CO_2–water–caprock interaction. The effect of salinity on the permeability of caprock was analyzed by increasing the water salinity in caprock in the Table 4. When the salinity was 0.10 (Fig. 10a) (the original formation water salinity), the dissolution depth of the caprock was slightly larger than that of 0.20 (Fig. 10b), indicating that the increase of salinity attenuated the CO_2 dissolution of the caprock and facilitated the sealing ability of the caprock. For further analysis, the increase of salinity led to the increase of the

concentration of ions in the caprock, and the synergistic effect of the ions was inhibited by the dissociation of the minerals, which would effectively reduce the dissolution effect of the caprock. However, from the results of this study, the salinity had little effect on the sealing of the mudstone caprock.

4 Discussion

Under the dual mechanisms of convection and diffusion, the supercritical CO_2 entered the caprock, making the concentration of dissolved CO_2 in the caprock change greatly. However, the supercritical CO_2 could not enter the caprock only under the diffusion mechanism, and the pH of the caprock water was affected within 2.3 m above the bottom of the caprock.

Different migration mechanisms of CO_2 in the caprock caused different changes in caprock permeability. The minerals that can precipitate as a result of high CO_2 content in water and the dissolution of primary minerals, such as kaolinite, quartz or chalcedony and carbonate minerals [39], while the kaolinite mainly dissolved and the quartz mainly precipitated, and the changes of quartz content in volume fraction during 5000 years were very small in our study. The dissolution of chlorite provided the necessary Mg^{2+} and Fe^{2+} for the precipitation of ankerite and magnesite, which played a crucial role in the increase of the caprock permeability [36, 40, 41], meanwhile the clay minerals that provide Mg^{2+} and Fe^{2+} to the system were also different in different stages [42]. However, this study has shown that the changes of Mg^{2+} and Fe^{2+} concentration have no obvious influence on the changes in caprock permeability under the diffusion mechanism. Dong *et al.* found that near the injection well, the increase of caprock bottom permeability was mainly caused by the dissolution of gypsum [31], while our results showed that the increase of caprock bottom permeability was mainly caused by the dissolution of K-feldspar and albite at a distance from the injection well. Gaus *et al.* also found that after several years of initial carbonate dissolution, feldspar dissolution dominates over the subsequent hundreds and thousands of years [43]. These studies will help to further understand the mechanism of caprock permeability variation under different migration mechanisms, especially under the diffusion mechanism.

Meanwhile, many studies have shown that the common-ion effect induced by increasing the formation water salinity inhibited the dissolution of the mineral, which can inhibit the dissolution of the caprock [44, 45]. However, under the diffusion mechanism the degree of inhibition was not obvious. Of course, under different mechanisms, the impacts of temperature on caprock permeability changes were consistent. Temperature increased the rate of increase of the caprock permeability, enhanced dissolution, because the kinetic reaction rate constants increase with increasing temperature. When the temperature increases, dissolution and precipitation rate of mineral increases [37, 38, 46].

Based on the above analysis, it can be seen that with different diffusion mechanisms of CO_2, the sealing mechanism and influencing factors of the caprock are also different. This study can provide a reference for the safety assessment of long-term CO_2 storage at a distance from the injection well (under the diffusion mechanism).

5 Conclusion

This study investigates the effect of supercritical CO_2–water–rock interactions, caprock mineralogy and reservoir conditions (temperature and salinity) on the seal capacity of caprock under the diffusion mechanism using TOUGHREACT based on the geological conditions of Jianghan Basin.

CO_2 gas did not enter the caprock under the diffusion mechanism, thus the amount of dissolved CO_2 in the caprock was very low compared to the case of convection + diffusion mechanism, which may have different effect on the caprock seal capacity between the diffusion and convection + diffusion mechanism. The dissolution proportion of the caprock at the bottom was larger than the convection + diffusion mechanism, the caprock permeability increased by 60% after 5000 years. The dissolution of the caprock gradually decreased from the bottom up to the top, and the dissolution range was only 2.3 m, which was mainly caused by the dissolution of K-feldspar and albite. In the absence of chlorite, K-feldspar and albite, the dissolution of the caprock decreased, indicating that the dissolution of the caprock was related to the dissolution of these three minerals and the effect of K-feldspar and albite was much larger than that of chlorite. These results could provide a theoretical basis for the safety evaluation of caprock in Jianghan Basin.

Temperature and salinity were other factors influencing the caprock permeability during CO_2–water–rock geochemical processes. The increase in caprock permeability increased with temperature because the kinetic reaction rate constants of the minerals increased with increasing temperature. The common-ion effect induced by increasing the formation water salinity inhibited the dissolution of the minerals, which would inhibit the dissolution of the caprock. However, the degree of inhibition in this study was very small.

This study focuses on the effect of CO_2–water–rock geochemical reactions on the change in caprock permeability under the diffusion mechanism (at a distance from the injection well), obtained the hereinafter conclusions. The results could do a favor to add the mineralogy of caprock and storage conditions into caprock evaluating system, and perfected it, provided theoretical according for caprock safety assessment, which benefited for the further research and widely development of related engineering of CO_2 geological sequestration in Jianghan Basin in the future.

Acknowledgments. This work was supported by the Project funded by National Natural Science Foundation of China (NSFC, Grant No. 41702284 and 41602272), the Initial Scientific Research Fund of Wuhan University of Science and Technology (Grant No. 620161) and the China Geological Survey (Grant No. DD20160307). We also would like to thank Dr. Liuqi WANG

(Geoscience Australia) for his guidance and help, which improve the quality of our work.

References

1 Katsoulidis A.P., Kanatzidis M.G. (2011) Phloroglucinol based microporous polymeric organic frameworks with −OH functional groups and high CO_2 capture capacity, *Chem. Mater.* **23**, 7, 1818–1824.

2 Tolón-Becerra A., Pérez-Martínez P., Lastra-Bravo X., Otero-Pastor I. (2012) A methodology for territorial distribution of CO_2, emission reductions in transport sector, *Int. J. Energy Res.* **36**, 14, 1298–1313.

3 Geough E.J.M., Little S.M., Janzen H.H., Mcallister T.A., Mcginn S.M., Beauchemin K.A. (2012) Life-cycle assessment of greenhouse gas emissions from dairy production in Eastern Canada: A case study, *J. Dairy Sci.* **95**, 9, 5164–5175.

4 Falcon-Suarez I., North L., Amalokwu K., Best A. (2016) Integrated geophysical and hydromechanical assessment for CO_2 storage: Shallow low permeable reservoir sandstones, *Geophys. Prospect.* **64**, 4, 828–847.

5 Rutqvist J. (2012) The geomechanics of CO_2 storage in deep sedimentary formations, *Geotech. Geol. Eng.* **30**, 3, 525–551.

6 Michael K., Golab A., Shulakova V., Ennis-King J., Allinson G., Sharma S., Aiken T. (2010) Geological storage of CO_2, in saline aquifers – A review of the experience from existing storage operations, *Int. J. Greenh. Gas Control.* **4**, 4, 659–667.

7 Celia M.A., Bachu S., Nordbotten J.M., Bandilla K.W. (2015) Status of CO_2 storage in deep saline aquifers with emphasis on modeling approaches and practical simulations, *Water Resour. Res.* **51**, 9, 6846–6892.

8 Li Q., Chen Z.A., Zhang J.T., Liu L.C., Li X.C., Jia L. (2016) Positioning and revision of CCUS technology development in China, *Int. J. Greenh. Gas Control.* **46**, 282–293.

9 Bachu S., Adams J.J. (2003) Sequestration of CO_2 in geological media in response to climate change: Capacity of deep saline aquifers to sequester CO_2 in solution, *Energy Convers. Manag.* **44**, 20, 3151–3175.

10 Bielicki J.M., Pollak M.F., Deng H., Wilson E.J., Fitts J.P., Peters C.A. (2016) The leakage risk monetization model for geologic CO_2 storage, *Environ. Sci. Technol.* **50**, 10, 4923–4931.

11 Dai Z.X., Viswanathan H., Middleton R., Pan F., Ampomah W., Yang C.B., Jia W., Xiao T., Lee S.Y., McPherson B., Balch R., Grigg R., White M. (2016) CO_2 accounting and risk analysis for CO_2 sequestration at enhanced oil recovery sites, *Environ. Sci. Technol.* **50**, 14, 7546–7554.

12 Yang G.D., Li Y.L., Atrens A., Liu D.Q., Wang Y.S., Jia L., Lu Y. (2017) Reactive transport modeling of long-term CO_2 sequestration mechanisms at the Shenhua CCS demonstration project, China, *J. Earth Sci.* **28**, 3, 457–472.

13 Siirila-Woodburn E.R., Cihan A., Birkholzer J.T. (2017) A risk map methodology to assess the spatial and temporal distribution of leakage into groundwater from Geologic Carbon Storage, *Int. J. Greenh. Gas Control.* **59**, 99–109.

14 Gherardi F., Xu T.F., Pruess K. (2007) Numerical modeling of self-limiting and self-enhancing caprock alteration induced by CO_2, storage in a depleted gas reservoir, *Chem. Geol.* **244**, 1–2, 103–129.

15 Nazari Moghaddam R., Rostami B., Pourafshary P. (2015) Scaling analysis of the convective mixing in porous media for geological storage of CO_2: An experimental approach, *Chem. Eng. Commun.* **202**, 6, 815–822.

16 Fujii T., Uehara S.I., Sorai M. (2015) Impact of effective pressure on threshold pressure of Kazusa Group Mudstones for CO_2 geological sequestration, *Mater. Trans.* **56**, 4, 519–528.

17 Uemura S., Matsui Y., Kondo F., Tsushima S., Hirai S. (2016) Injection of nanosized CO_2 droplets as a technique for stable geological sequestration, *Int. J. Greenh. Gas Control.* **45**, 62–69.

18 Li Q., Liu G.Z., Liu X.H., Li X.C. (2013) Application of a health, safety, and environmental screening and ranking framework to the Shenhua CCS project, *Int. J. Greenh. Gas Control.* **17**, 5, 504–514.

19 Wang F.G., Mi Z.X., Sun Z.J., Li X.F., Lan T.S., Yuan Y., Xu T.F. (2017) Experimental study on the effects of stress variations on the permeability of feldspar-quartz sandstone, *Geofluids* **2017**, 3, 1–15.

20 Xie J., Zhang K.N., Wang Y.S., Qin L.Q., Guo C.B. (2016) Performance assessment of CO_2 geological storage in deep saline aquifers in Ordos Basin, China, *Rock Soil Mech.* **37**, 1, 166–174. (in Chinese with English abstract).

21 Luquot L., Gouze P. (2009) Experimental determination of porosity and permeability changes induced by injection of CO_2 into carbonate rocks, *Chem. Geol.* **265**, 1–2, 148–159.

22 Bacon D.H., Dai Z., Zheng L. (2014) Geochemical impacts of carbon dioxide, brine, trace metal and organic leakage into an unconfined, oxidizing limestone aquifer, *Energy Procedia* **63**, 4684–4707.

23 Wolf J.L., Niemi A., Bensabat J., Rebscher D. (2016) Benefits and restrictions of 2D reactive transport simulations of CO_2 and SO_2 co-injection into a saline aquifer using TOUGHREACT V3.0-OMP, *Int. J. Greenh. Gas Control.* **54**, 610–626.

24 Roded R., Paredes X., Holtzman R. (2018) Reactive transport under stress: Permeability evolution in deformable porous media, *Earth Planet. Sci. Lett.* **493**, 198–207.

25 Wang Y., Zhang L., Soong Y., Dilmore R., Liu H., Lei H., Li X. (2019) From core-scale experiment to reservoir-scale modeling: A scale-up approach to investigate reaction-induced permeability evolution of CO_2 storage reservoir and caprock at a U.S. CO_2 storage site, *Comput. Geosci.* **125**, 55–68.

26 Soong Y., Howard B.H., Dilmore R.M., Haljasmaa I., Crandall D.M., Zhang L.W., Zhang W., Lin R.H., Irdi G. A., Romanov V.N., Mclendon T.R. (2016) CO_2/brine/rock interactions in lower Tuscaloosa formation, *Greenh. Gases: Sci. Technol.* **6**, 6, 824–837.

27 Guo J.Q., Wen D.G., Zhang S.Q., Xu T.F. (2014), *Potential evaluation and project of CO_2 geological storage in china*, Geological Publishing House, Beijing, China, pp. 69–81.

28 Xu T.F., Pruess K. (1998) *Coupled modeling of non-isothermal multiphase flow, solute transport and reactive chemistry in porous and fractured media: 1. Model development and validation*, Lawrence Berkeley National Laboratory Report LBNL-42050, Berkeley, CA, p. 38.

29 Xu T.F., Spycher N., Sonnenthal E., Zhang G.X., Zheng L. G., Pruess K. (2011) Toughreact version 2.0: A simulator for subsurface reactive transport under non-isothermal multiphase flow conditions, *Comput. Geosci.* **37**, 6, 763–774.

30 Xu T.F., Sonnenthal E., Spycher N., Pruess K. (2006) TOUGHREACT – A simulation program for non-isothermal multiphase reactive geochemical transport in variably

saturated geologic media: Applications to geothermal injectivity and CO_2, geological sequestration, *Comput. Geosci.* **32**, 2, 145–165.

31 Dong J.X., Li Y.L., Yang G.D., Ke Y.B., Wu R.H. (2012) Numerical simulation of CO_2-water-rock interaction impact on caprock permeability, *Geol. Sci. Technol. Inf.* **31**, 1, 119–125. (in Chinese with English abstract).

32 Guo Z.F., Hu X.F., Cui C. (2004) Affecting factors of Cretaceous-Paleogene shale cap in Jianghan Plain, *J. Jianghan Pet. Univ. Staff Work.* **17**, 2, 10–13. (in Chinese with English abstract).

33 Zheng Y., Chen S.L., Zhang W., Xiong P., Jiang L., Qiu G. B., Wang H. (2009) Numerical simulation on geological storage of carbon dioxide in Jiangling depression, Jianghan Basin, China, *Geol. Sci. Technol. Inf.* **28**, 4, 75–82. (in Chinese with English abstract).

34 Petroleum Geology Group of Jianghan Oilfield (1991) *Petroleum geology of China (Vol. 9): Jianghan oilfield*, Petroleum Industry Press, Beijing, China, pp. 157–204.

35 Xu T.F., Apps J.A., Pruess K., Yamamoto H. (2007) Numerical modeling of injection and mineral trapping of CO_2 with H_2S and SO_2 in a sandstone formation, *Chem. Geol.* **242**, 3–4, 319–346.

36 Zhang W., Li Y., Xu T.F., Cheng H.L., Zheng Y., Xiong P. (2009) Long-term variations of CO_2 trapped in different mechanisms in deep saline formations: A case study of the Songliao Basin, China, *Int. J. Greenh. Gas Control.* **3**, 2, 161–180.

37 Lasaga A.C., Soler J.M., Ganor J., Burch T.E., Nagy K.L. (1994) Chemical weathering rate laws and global geochemical cycles, *Geochim. Cosmochim. Acta* **58**, 10, 2361–2386.

38 Xu T.F., Sonnenthal E., Spycher N., Pruess K. (2003) *TOUGHREACT User's guide: A simulation program for non-isothermal multiphase reactive geochemical transport in variably saturated geological media*, Lawrence Berkeley National Laboratory, Berkeley, California, pp. 148−157.

39 Joachim T., Castillo C., Vong C.Q., Christophe K., Lassin A., Audigane P. (2014) Long-term assessment of geochemical reactivity of CO_2 storage in highly saline aquifers: Application to ketzin, in salah and snøhvit storage sites, *Int. J. Greenh. Gas Control.* **20**, 3, 2–26.

40 Tian H.L., Pan F., Tianfu XuTF, McPherson B.J., Yue G.F., Mandalaparty P. (2014) Impacts of hydrological heterogeneities on caprock mineral alteration and containment of CO_2 in geological storage sites, *Int. J. Greenh. Gas Control.* **24**, 30–42.

41 Wang K.R., Xu T.F., Tian H.L., Wang F.G. (2016) Impacts of mineralogical compositions on different trapping mechanisms during long-term CO_2 storage in deep saline aquifers, *Acta Geotech.* **11**, 5, 1167–1188.

42 Tian H.L., Xu T.F., Wang F.G., Patil V.V., Sun Y., Yue G.F. (2014) A numerical study of mineral alteration and self-sealing efficiency of a caprock for CO_2 geological storage, *Acta Geotech.* **9**, 1, 87–100.

43 Gaus I., Azaroual M., Czernichowski-Lauriol I. (2005) Reactive transport modeling of the impact of CO_2 injection on the clayey cap rock at Sleipner (North Sea), *Chem. Geol.* **217**, 3–4, 319–337.

44 Ke Y.B., Li Y.L., Zhang W., Dong J.X., Fang Q., Wu R.H. (2012) Impact of halite precipitation on CO_2 injection into saline aquifers: A case study of Jianghan Basin, *Geol. Sci. Technol. Inf.* **31**, 3, 109–115. (in Chinese with English abstract).

45 Li Y.L., Fang Q., Ke Y.B., Dong J.X., Yang G.D., Ma X. (2012) Effect of high salinity on CO_2 geological storage: A case study of Qianjiang depression in Jianghan Basin, *Earth Sci. J. China Univ. Geosci.* **37**, 2, 109–115. (in Chinese with English abstract).

46 Smith M.M., Wolery T.J., Carroll S.A. (2013) Kinetics of chlorite dissolution at elevated temperatures and CO_2 conditions, *Chem. Geol.* **347**, 1–8.